

Topological Scaling of Nonlinear Injection current and the Quantized Circular Photogalvanic Effect (CPGE) in tilted multi Weyl semimetals (mWSMs)

Deepannita Das and Alestin Mawrie

Department of Physics, Indian Institute of Technology Indore, Simrol, Indore-453552, India

(Dated: February 18, 2026)

We develop a microscopic theory of nonlinear magneto-optical injection currents in multi-Weyl semimetals subjected to a uniform magnetic field. Using the Landau-level spectrum of a tilted multi-Weyl Hamiltonian with arbitrary monopole charge ν as a starting point, we formulate a Kubo-type nonlinear response theory in the Landau-level basis and derive the second-order conductivity tensor. We identify distinct contributions originating from chiral-chiral, chiral-bulk, and bulk-bulk optical transitions, revealing characteristic monopole-charge scaling and sharp resonant structures governed by Landau-level selection rules and tilt-induced asymmetry. In the untilted limit, closed-form analytical expressions emerge that expose universal frequency thresholds and provide clear experimental signatures of higher-order Weyl topology. Our results establish nonlinear magneto-optical injection currents as a direct transport probe of chiral Landau levels and multi-Weyl topological charge.

I. INTRODUCTION

Weyl semimetals constitute a paradigmatic class of topological quantum matter in which low-energy quasi-particles realize Weyl fermions and the electronic bands host monopoles of Berry curvature^{1–6}. The associated Weyl nodes carry an integer topological charge (chirality), leading to striking phenomena such as Fermi-arc surface states, anomalous Hall responses, and the chiral anomaly in the presence of electromagnetic fields^{7–12}. These properties establish Weyl systems as an important platform for studying the interplay of topology, symmetry, and electromagnetic response¹³. Beyond conventional Weyl semimetals with unit monopole charge, crystalline symmetries can stabilize *multi-Weyl semimetals*, where Weyl nodes possess higher topological charge $\nu > 1$, and exhibit nonlinear transverse dispersion^{14–17}. In such systems, the dispersion remains linear along one momentum direction but becomes quadratic or cubic in the transverse plane, resulting in enhanced Berry curvature effects and unconventional scaling of physical observables with external fields¹⁸. A particularly important consequence is the emergence of multiple topologically protected chiral Landau levels in a magnetic field, directly reflecting the monopole charge of the Weyl node.

Nonlinear optical and transport phenomena have recently emerged as sensitive probes of electronic topology and quantum geometry, enabling direct experimental access to Berry curvature, Berry connection, and topological charge via observables such as shift and injection photocurrents and nonlinear Hall responses^{15,19–24}. While linear transport is often dominated by scattering mechanisms and the density of states, nonlinear responses directly encode Berry curvature and interband coherence. In noncentrosymmetric systems, second-order effects such as the nonlinear Hall effect arise from the Berry curvature dipole⁶, providing a purely geometric contribution to nonlinear transport. Similarly, nonlinear photocurrents such as the circular photogalvanic effect (CPGE) and injection currents have been predicted

to reveal Weyl-node chirality and topological charge^{15,24}. These theoretical developments have been accompanied by experimental observations of nonlinear photocurrents in Weyl materials. In particular, signatures of CPGE have been reported in TaAs-family Weyl semimetals²³, and strong quantized-like responses have been observed in structurally chiral multifold semimetals such as RhSi and CoSi^{25,26}. These experiments demonstrate that nonlinear optical probes provide direct access to topological information that may be obscured in conventional linear measurements⁸.

The application of a magnetic field introduces an additional layer of richness. Landau quantization discretizes the spectrum into bulk Landau levels while generating chiral Landau levels that act as topologically protected one-dimensional channels^{11,18}. Such chiral modes are central to magnetotransport and anomaly-related physics, and they are expected to play a prominent role in nonlinear optical processes in strong fields. Although linear magneto-optical responses of Weyl and Dirac systems have been widely explored, including Kerr and Faraday effects^{27–29}, the nonlinear magneto-optical response of multi-Weyl semimetals remains much less understood. In particular, the second-order *injection current* generated by resonant inter-Landau-level transitions in the presence of a magnetic field has not been systematically investigated for higher monopole charge^{24,30}. Injection currents arise from asymmetric carrier population following optical excitation and are inherently sensitive to Landau-level selection rules³¹, current matrix elements, and the presence of chiral channels. The interplay of multi-Weyl topology, chiral Landau levels, and band tilting is therefore expected to produce pronounced and experimentally accessible fingerprints in nonlinear magneto-optical response^{32,33}.

In this work, we develop a microscopic theory of nonlinear magneto-optical injection currents in multi-Weyl semimetals subjected to a uniform magnetic field. Starting from a tilted multi-Weyl Hamiltonian with arbitrary monopole charge ν , and using the known complete Landau-level spectrum we evaluate the second-order con-

ductivity tensor using a Kubo-type nonlinear response formalism^{3,34}. We show that the injection current naturally decomposes into distinct chiral-chiral, chiral-bulk, and bulk-bulk contributions, each exhibiting characteristic monopole-charge scaling and optical resonances. In the untilting limit, we obtain closed-form analytical expressions revealing universal frequency thresholds and providing clear signatures of higher-order Weyl topology.

The remainder of this paper is organized as follows. Section II introduces the model Hamiltonian and Landau-level spectrum. Section III develops the nonlinear response formalism and provides a detailed analysis of chiral and bulk contributions to the injection current, together with the untilted limit and the associated universal scaling behavior. Section IV summarizes our conclusions.

II. MODEL HAMILTONIAN AND LANDAU-LEVEL SPECTRUM

We perform our analysis for multi-Weyl semimetals (mWSMs). We begin by considering the low-energy Hamiltonian near a Weyl node in the absence of an external magnetic field^{13,35,36}.

$$\mathcal{H}_0(\mathbf{k}) = \left(k_z + \eta \frac{\mathcal{K}}{2} \right) (t_z \sigma_0 + \eta v_z \sigma_z) + \lambda (k_-^\nu \sigma_+ + k_+^\nu \sigma_-), \quad (1)$$

where $\mathbf{k} = (k_x, k_y, k_z)$ is the crystal momentum measured from the Weyl node located at $\mathbf{k} = (0, 0, \eta\mathcal{K}/2)$. Here, ν denotes the monopole charge (Weyl-node order), λ characterizes the multi-Weyl coupling strength, v_z is the Fermi velocity along the z direction, t_z represents the tilt of the Weyl cone along z , $\sigma_{x,y,z}$ are Pauli matrices in pseudospin space, and $\eta = \pm 1$ labels the chirality of the Weyl node. We have defined $k_\pm = k_x \pm ik_y$.

We now introduce a uniform magnetic field $\mathbf{B} = B_0 \hat{z}$ and choose the Landau gauge $\mathbf{A} = (0, B_0 x, 0)$. In the presence of the magnetic field, the Hamiltonian near the Weyl node takes the form¹³

$$\mathcal{H} = \left(k_z + \eta \frac{\mathcal{K}}{2} \right) (t_z \sigma_0 + \eta v_z \sigma_z) + t_{\parallel} (2\hat{a}^\dagger \hat{a} + 1) \sigma_0 + \varepsilon_B \begin{pmatrix} 0 & \hat{a}^\nu \\ (\hat{a}^\dagger)^\nu & 0 \end{pmatrix}, \quad (2)$$

where \hat{a}^\dagger and \hat{a} are the Landau-level creation and annihilation operators. The magnetic energy scale is given by $\varepsilon_B = \lambda (\sqrt{2}/\ell_B)^\nu$, with $\ell_B = \sqrt{\hbar/(eB_0)}$ being the magnetic length. The parameter t_{\parallel} denotes the in-plane tilt, which lifts the degeneracy of the chiral Landau levels.

Winding number	v_z (eV Å)	t_z (eV Å)	t_{\parallel} (eV Å 2)	λ (eV Å $^\nu$)
$\nu = 1$	1	$0.5 v_z$	0.03	0.4
$\nu = 2$	1.5	$0.5 v_z$	0.2	0.2
$\nu = 3$	2	$0.5 v_z$	0.2	0.1

TABLE I. Model parameters used in this work are chosen within experimentally measured and first-principles-calculated ranges for Weyl and multi-Weyl semimetals. For $m = 1$, band velocities and tilt strengths follow ARPES and *ab initio* studies of TaAs and NbP^{37–39}. For $m = 2$, the nonlinear dispersion parameter λ and anisotropy v_z/λ are consistent with double-Weyl candidates such as SrSi₂⁴⁰. For $m = 3$, enhanced anisotropy and nonlinear coefficients reflect cubic Weyl dispersions observed in multifold chiral crystals like CoSi and RhSi^{41,42}. Overall, the adopted dimensionless ratios w_z/v_z , λ , and w_{\parallel} lie within realistic material ranges, ensuring quantitative relevance to experimentally accessible multi-Weyl systems.

1. Bulk Landau levels ($n \geq \nu$)

For Landau-level indices $n \geq \nu$, the spectrum consists of bulk (nonchiral) Landau levels with two-component pseudospin structure. The corresponding eigenstates are

$$|n, k_z, s\rangle = \begin{pmatrix} u_{n,\uparrow}^s(k_z) |n - \nu\rangle \\ u_{n,\downarrow}^s(k_z) |n\rangle \end{pmatrix}, \quad (3)$$

where $|n\rangle$ denotes the n th harmonic-oscillator state and $s = \pm 1$ labels the band index. The spinor components are given by

$$\left. \begin{aligned} u_{n,\uparrow}^s(k_z) &= \frac{1}{\sqrt{2}} \sqrt{1 - s \frac{\nu t_{\parallel} - v_z \eta (k_z + \eta \frac{\mathcal{K}}{2})}{\Gamma_n^\nu(k_z)}}, \\ u_{n,\downarrow}^s(k_z) &= \frac{1}{\sqrt{2}} \sqrt{1 + s \frac{\nu t_{\parallel} - v_z \eta (k_z + \eta \frac{\mathcal{K}}{2})}{\Gamma_n^\nu(k_z)}}. \end{aligned} \right\} \quad (4)$$

The corresponding energy eigenvalues for $n \geq \nu$ are

$$\varepsilon_{n,s}^{\text{bulk}}(k_z) = (2n - \nu + 1) t_{\parallel} + t_z \left(k_z + \eta \frac{\mathcal{K}}{2} \right) + s \Gamma_n^\nu(k_z), \quad (5)$$

where

$$\Gamma_n^\nu(k_z) = \sqrt{\left[-\nu t_{\parallel} + v_z \eta \left(k_z + \eta \frac{\mathcal{K}}{2} \right) \right]^2 + \varepsilon_B^2 \frac{n!}{(n - \nu)!}}. \quad (6)$$

2. Chiral Landau levels ($n < \nu$)

For $n < \nu$, the system hosts chiral Landau levels originating from the nontrivial monopole charge ν . In this case, only a single pseudospin component survives, and

the eigenstates reduce to $|n, k_z\rangle = (0 \ |n\rangle)'$, with ' denoting the transpose. The corresponding energy dispersion is linear in k_z and is given by

$$\varepsilon_n^{\text{ch}}(k_z) = \left(k_z + \eta \frac{\mathcal{K}}{2} \right) (-\eta v_z + t_z) + (2n + 1)t_{\parallel}. \quad (7)$$

These chiral Landau levels are unidirectional, with their propagation direction determined by the Weyl-node chirality η , and are insensitive to the magnetic energy scale ε_B , reflecting their topological origin.

III. NONLINEAR CURRENT RESPONSE

We consider the system to be under a time-dependent electric field of the form $\mathbf{E}(t) = \mathbf{E}_0 e^{i\Omega t}$, where Ω denotes the frequency of the generated current. The most general form of the second-order electrical current density generated in response to an external electromagnetic field can be expressed in terms of the third-rank nonlinear conductivity tensor $\sigma^{\alpha\beta\gamma}(\omega, \Omega - \omega)$ as²¹

$$j^{\gamma}(\Omega) = \sigma^{\alpha\beta\gamma}(i\omega, i(\Omega - \omega)) E^{\alpha}(\omega) E^{\beta}(\Omega - \omega), \quad (8)$$

where $\Omega = \omega_1 + \omega_2$ denotes the output frequency arising from the mixing of two incident fields at frequencies ω_1 and ω_2 . Here, $E^{\alpha}(\omega_i)$ represents the α -component of the applied electric field oscillating at frequency ω_i , while $j^{\gamma}(\Omega)$ denotes the γ -component of the induced photocurrent. Physically, the nonlinear conductivity tensor encodes how the combined action of two electric-field components along directions α and β produces a current along direction γ .

The second-order conductivity tensor can be written in terms of a three-point nonlinear correlation function as^{34,43,44}

$$\sigma^{\alpha\beta\gamma}(i\omega_1, i\omega_2) = \frac{\chi^{\alpha\beta\gamma}(i\omega_1, i\omega_2) + \chi^{\beta\alpha\gamma}(i\omega_2, i\omega_1)}{i\omega_1 i\omega_2}, \quad (9)$$

which explicitly symmetrizes the response with respect to the two incoming fields, reflecting their physical equivalence in the nonlinear process.

The nonlinear correlation function $\chi^{\alpha\beta\gamma}$ is defined as

$$\begin{aligned} \chi^{\alpha\beta\gamma}(i\omega_1, i\omega_2) &= \frac{1}{V} \int \frac{d\varepsilon}{2\pi} \text{Tr} \left[\hat{j}^{\alpha} G(i\varepsilon - i\omega_1) \right. \\ &\quad \times \left. \hat{j}^{\beta} G(i\varepsilon - i\Omega) \hat{j}^{\gamma} G(i\varepsilon) \right], \end{aligned} \quad (10)$$

where V denotes the system volume. The trace implies summation over all internal quantum numbers, including the Landau-level index n , the band index $s = \pm 1$ for bulk Landau levels, the momentum k_z , and pseudospin degrees of freedom⁴⁵. This three-point correlation function represents the quantum-amplitude for a process in which an electron sequentially interacts with two electric fields and contributes to a current response.

In systems possessing inversion or certain mirror symmetries, the above correlation function vanishes identically⁶. In the present case, however, the presence of tilt parameters breaks these symmetries of the Weyl node, rendering $\chi^{\alpha\beta\gamma}$ finite and allowing a nonvanishing second-order current response.

The Green's function appearing above acts as the propagator of the system and is written in the eigenstate basis as

$$G(\omega; \mathbf{r}_1, \mathbf{r}_2) = \sum_{n, s, k_z} \frac{|\Psi_{n, s, k_z}(\mathbf{r}_1)\rangle \langle \Psi_{n, s, k_z}(\mathbf{r}_2)|}{\hbar\omega + i\eta - \varepsilon_{n, s}(k_z) + \mu}, \quad (11)$$

where $|\Psi_{n, s, k_z}\rangle$ are the eigenstates of the Hamiltonian, $\varepsilon_{n, s}(k_z)$ are the corresponding Landau-level energies, μ is the chemical potential, and the infinitesimal parameter $\eta \rightarrow 0^+$ ensures causality. For chiral Landau levels ($n < \nu$), the band index s is absent.

The coupling between the electronic system and the external electric field is mediated by the current density operator

$$\hat{j}^{\alpha} = -\frac{e}{\hbar} \frac{\partial \mathcal{H}}{\partial k_{\alpha}}, \quad (12)$$

where $\alpha = x, y, z$ labels the spatial components. This definition follows directly from the minimal-coupling prescription and identifies the current operator with the band velocity.

Starting from the general three-point current correlation function and performing the Matsubara-frequency integration, the nonlinear response kernel can be expressed explicitly in the Landau-level basis³⁴. After evaluating the trace over internal degrees of freedom, the second-order correlation function takes the form

$$\begin{aligned} \chi^{\alpha\beta\gamma}(i\omega_1, i\omega_2) &= \frac{e^3 \eta}{2\pi \ell_B^2} \sum_{\xi_1, \xi_2, \xi_3} \frac{\mathcal{Z}_{\xi_1 \xi_2 \xi_3}^{\alpha\beta\gamma}}{i\hbar\omega_1 + \varepsilon_{\xi_1} - \varepsilon_{\xi_2}} \\ &\quad \times \frac{\Theta(\varepsilon_{\xi_2}) - \Theta(\varepsilon_{\xi_1})}{i\omega_2 + \varepsilon_{\xi_2} - \varepsilon_{\xi_1}}. \end{aligned} \quad (13)$$

Here, $\Theta(\varepsilon_{\xi_i}) \equiv \Theta(\varepsilon_{\xi_i} - \mu)$ denotes the Fermi step function corresponding to an energy level ε_{ξ_i} ⁶. The prefactor $(2\pi \ell_B^2)^{-1}$ reflects the Landau-level degeneracy. The summation runs over all quantum numbers, where $\xi_i \equiv (s_i, n_i, k_{z,i})$. The triple current matrix element is defined as

$$\mathcal{Z}_{\xi_1 \xi_2 \xi_3}^{\alpha\beta\gamma} = \langle \Psi_{\xi_3} | \hat{j}^{\alpha} | \Psi_{\xi_1} \rangle \langle \Psi_{\xi_1} | \hat{j}^{\beta} | \Psi_{\xi_2} \rangle \langle \Psi_{\xi_2} | \hat{j}^{\gamma} | \Psi_{\xi_3} \rangle. \quad (14)$$

To extract the physically relevant nonlinear response, we perform analytic continuation according to^{6,34} $i\omega_1 \rightarrow \omega + \Omega + i0^+$, $i\omega_2 \rightarrow -\omega + i0^+$.

$$\begin{aligned} \chi^{\alpha\beta\gamma}(\omega + \Omega, -\omega) &= \frac{e^3 \eta}{2\pi \ell_B^2} \sum_{\xi_1, \xi_2, \xi_3} \frac{\mathcal{Z}_{\xi_1 \xi_2 \xi_3}^{\alpha\beta\gamma}}{-\hbar\omega + i0^+ + \varepsilon_{\xi_2} - \varepsilon_{\xi_1}} \\ &\quad \times \frac{\Theta(\varepsilon_{\xi_2}) - \Theta(\varepsilon_{\xi_1})}{\hbar\omega + \hbar\Omega + i0^+ + \varepsilon_{\xi_1} - \varepsilon_{\xi_2}}. \end{aligned} \quad (15)$$

Using the identity $\frac{1}{x+i0^+} = \mathcal{P}(1/x) - i\pi\delta(x)$, we obtain

$$\chi^{\alpha\beta\gamma}(\omega + \Omega, -\omega) = \frac{\eta}{2\pi\ell_B^2} \sum_{\xi_1, \xi_2, \xi_3} \frac{[\Theta(\varepsilon_{\xi_2}) - \Theta(\varepsilon_{\xi_1})] \mathcal{Z}_{\xi_1\xi_2\xi_3}^{\alpha\beta\gamma}}{\hbar\omega + \hbar\Omega + i0^+ + \varepsilon_{\xi_1} - \varepsilon_{\xi_2}} \left[\mathcal{P}\left(\frac{1}{-\hbar\omega + \varepsilon_{\xi_2} - \varepsilon_{\xi_1}}\right) - i\pi\delta(-\hbar\omega + \varepsilon_{\xi_2} - \varepsilon_{\xi_1}) \right]. \quad (16)$$

Similarly,

$$\chi^{\beta\alpha\gamma}(-\omega, \omega + \Omega) = \frac{\eta}{2\pi\ell_B^2} \sum_{\xi_1, \xi_2, \xi_3} \frac{[\Theta(\varepsilon_{\xi_2}) - \Theta(\varepsilon_{\xi_1})] \mathcal{Z}_{\xi_1\xi_2\xi_3}^{\beta\alpha\gamma}}{-\hbar\omega + i0^+ + \varepsilon_{\xi_1} - \varepsilon_{\xi_2}} \left[\mathcal{P}\left(\frac{1}{\hbar\omega + \hbar\Omega + \varepsilon_{\xi_2} - \varepsilon_{\xi_1}}\right) - i\pi\delta(\hbar\omega + \hbar\Omega + \varepsilon_{\xi_2} - \varepsilon_{\xi_1}) \right]. \quad (17)$$

Adding Eqs. (16) and (17), the principal parts cancel, yielding

$$\begin{aligned} & \chi^{\alpha\beta\gamma}(\omega + \Omega, -\omega) + \chi^{\beta\alpha\gamma}(-\omega, \omega + \Omega) \\ &= -\frac{i\eta}{2\ell_B^2 \Omega} \sum_{\xi_1, \xi_2, \xi_3} [\Theta(\varepsilon_{\xi_2}) - \Theta(\varepsilon_{\xi_1})] \\ & \quad \times [\mathcal{Z}_{\xi_1\xi_2\xi_3}^{\alpha\beta\gamma} \delta(\varepsilon_{\xi_2} - \varepsilon_{\xi_1} - \hbar\omega) \\ & \quad + \mathcal{Z}_{\xi_1\xi_2\xi_3}^{\beta\alpha\gamma} \delta(\hbar\omega + \hbar\Omega + \varepsilon_{\xi_2} - \varepsilon_{\xi_1})]. \end{aligned} \quad (18)$$

The nonlinear conductivity tensor in Eq. [9] now becomes

$$\begin{aligned} & \sigma^{\alpha\beta\gamma}(\omega + \Omega, -\omega) = -\frac{i\eta}{2\ell_B^2 \Omega(\Omega + \omega)(-\omega)} \\ & \quad \times \sum_{\xi_1, \xi_2, \xi_3} [\Theta(\varepsilon_{\xi_2}) - \Theta(\varepsilon_{\xi_1})] [\mathcal{Z}_{\xi_1\xi_2\xi_3}^{\alpha\beta\gamma} \delta(\varepsilon_{\xi_2} - \varepsilon_{\xi_1} - \hbar\omega) \\ & \quad + \mathcal{Z}_{\xi_1\xi_2\xi_3}^{\beta\alpha\gamma} \delta(\hbar\omega + \hbar\Omega + \varepsilon_{\xi_2} - \varepsilon_{\xi_1})]. \end{aligned} \quad (19)$$

Equation (19) represents the general second-order nonlinear conductivity evaluated at a finite output frequency Ω . The prefactor $[\Omega(\Omega + \omega)(-\omega)]^{-1}$ ^{43,46} originates from the frequency denominators of the three-point current correlation function²¹ and encodes the dynamical nature of the nonlinear optical response. In particular, the Dirac delta functions enforce energy conservation for photon absorption and emission processes between Landau levels, while the difference of Fermi functions selects only transitions between occupied and unoccupied states.

The physically relevant quantity for the injection current corresponds to the *dc limit* of the nonlinear response, obtained by taking the limit $\Omega \rightarrow 0$ while keeping the incoming photon frequency ω finite^{43,46}. In this limit, the factor $[\Omega(\Omega + \omega)(-\omega)]^{-1}$ reduces to $1/\omega^2$, and the second delta function simplifies according to $\delta(\hbar\omega + \hbar\Omega + \varepsilon_{\xi_2} - \varepsilon_{\xi_1}) \rightarrow \delta(\hbar\omega + \varepsilon_{\xi_2} - \varepsilon_{\xi_1})$ ⁴⁷. As a result, the nonlinear conductivity tensor reduces to the injection tensor $\beta^{\alpha\beta\gamma}(\omega)$, which characterizes the rate of dc current generation induced by resonant optical transitions.

$$\begin{aligned} & \beta^{\alpha\beta\gamma}(\omega) = \frac{\eta}{2\ell_B^2 \omega^2} \sum_{\xi_1, \xi_2, \xi_3} [\Theta(\varepsilon_{\xi_2}) - \Theta(\varepsilon_{\xi_1})] \\ & \quad \times [\mathcal{Z}_{\xi_1\xi_2\xi_3}^{\alpha\beta\gamma} \delta(\varepsilon_{\xi_2} - \varepsilon_{\xi_1} - \hbar\omega) + \mathcal{Z}_{\xi_1\xi_2\xi_3}^{\beta\alpha\gamma} \delta(\hbar\omega + \varepsilon_{\xi_2} - \varepsilon_{\xi_1})] \end{aligned} \quad (20)$$

We will eventually end up defining the quantities $\text{Re}[\beta_{xxz}]$ and $\text{Im}[\beta_{xyz}]$ based on the nature of the triple current matrix elements. In particular, the symmetry properties and phase structure of these matrix elements determine whether

the corresponding nonlinear response coefficients acquire predominantly real or imaginary contributions. Since the three-current correlation involves products of interband velocity operators, different combinations of matrix elements can either preserve or break time-reversal-like phase relations, leading to distinct dispersive and absorptive parts of the response. As a result, $\text{Re}[\beta_{xxz}]$ is associated mainly with the reactive (dispersive) component of the nonlinear conductivity, whereas $\text{Im}[\beta_{xyz}]$ captures the dissipative or absorptive behavior. This separation becomes especially important when analyzing magneto-optical effects, where the interplay between chiral Landau levels and higher-energy bulk states governs the overall nonlinear optical response.

A. Chiral-chiral contribution to the injection current

We first analyze the contribution to the injection current arising purely from transitions between chiral Landau levels. These modes originate from the topologically protected zeroth Landau levels and disperse linearly along the magnetic-field direction, making them particularly relevant for nonlinear optical response²⁹.

For the chiral Landau-level states described by Eq. (7), the current-operator matrix elements acquire a particularly simple structure defined in Eq. (21). The transverse components originate entirely from the tilt-induced terms in the Hamiltonian, whereas the longitudinal component is determined by the chirality-dependent group velocity along the magnetic-field direction^{32,33}. The nonvanishing matrix elements are therefore given by

$$\left. \begin{aligned} \langle n_3 | \hat{j}^x | n_1 \rangle &= \frac{\sqrt{2}\ell_B}{\hbar} t_{\parallel} (\sqrt{n_1} \delta_{n_3, n_1-1} + \sqrt{n_1+1} \delta_{n_3, n_1+1}), \\ \langle n_3 | \hat{j}^y | n_1 \rangle &= i \frac{\sqrt{2}\ell_B}{\hbar} t_{\parallel} (\sqrt{n_1} \delta_{n_3, n_1-1} - \sqrt{n_1+1} \delta_{n_3, n_1+1}), \\ \langle n_3 | \hat{j}^z | n_1 \rangle &= (t_z - v_z \eta) \delta_{n_1, n_3}. \end{aligned} \right\} \quad (21)$$

Using these matrix elements, the triple-current correlators entering the nonlinear conductivity tensor can be evaluated

explicitly. One obtains

$$\begin{aligned} \mathcal{Z}_{n_1 n_2 n_3}^{xxz} &= e^3 \left(\sqrt{2} t_{\parallel} \frac{\ell_B}{\hbar} \right)^2 (t_z - v_z \eta) [n_1 \delta_{n_2, n_1 - 1} \\ &\quad + (n_1 + 1) \delta_{n_2, n_1 + 1}] \delta_{n_2, n_3}, \end{aligned} \quad (22)$$

$$\begin{aligned} \mathcal{Z}_{n_1 n_2 n_3}^{xyz} &= ie^3 \left(\sqrt{2} t_{\parallel} \frac{\ell_B}{\hbar} \right)^2 (t_z - v_z \eta) [n_1 \delta_{n_2, n_1 - 1} \\ &\quad - (n_1 + 1) \delta_{n_2, n_1 + 1}] \delta_{n_2, n_3}. \end{aligned} \quad (23)$$

The Kronecker delta functions enforce strict dipole selec-

tion rules, restricting optical transitions to adjacent chiral Landau levels only³¹. Consequently, the chiral-chiral contribution to the injection current is highly resonant and depends sensitively on both the Weyl-node chirality and the tilt parameters. This term therefore constitutes the leading topological component of the nonlinear magneto-optical response in the presence of a magnetic field^{15,20}.

Substituting the chiral-chiral matrix elements into the general expression for the injection current tensor²¹ in Eq. ((20)), the β^{xxz} and β^{xyz} component takes the form

$$\begin{aligned} \beta^{xxz}(\omega) &= \frac{e^3 \eta}{2\pi \ell_B^2 \omega^2} \left(t_{\parallel} \frac{\ell_B}{\hbar} \right)^2 \sum_{n=0}^{\nu-1} \int_{-\infty}^{\infty} dk_z (t_z - v_z \eta) \{ n [\Theta(\varepsilon_{n-1}^{\text{ch}}) - \Theta(\varepsilon_n^{\text{ch}})] [\delta(\varepsilon_{n-1}^{\text{ch}} - \varepsilon_n^{\text{ch}} - \omega) + \delta(\omega + \varepsilon_{n-1}^{\text{ch}} - \varepsilon_n^{\text{ch}})] \\ &\quad + (n+1) [\Theta(\varepsilon_{n+1}^{\text{ch}}) - \Theta(\varepsilon_n^{\text{ch}})] [\delta(\varepsilon_{n+1}^{\text{ch}} - \varepsilon_n^{\text{ch}} - \omega) + \delta(\omega + \varepsilon_{n+1}^{\text{ch}} - \varepsilon_n^{\text{ch}})] \}. \end{aligned} \quad (24)$$

$$\begin{aligned} \beta^{xyz}(\omega) &= i \frac{e^3 \eta}{2\pi \ell_B^2 \omega^2} \left(t_{\parallel} \frac{\ell_B}{\hbar} \right)^2 \sum_{n=0}^{\nu-1} \int_{-\infty}^{\infty} dk_z (t_z - v_z \eta) \{ n [\Theta(\varepsilon_{n-1}^{\text{ch}}) - \Theta(\varepsilon_n^{\text{ch}})] [\delta(\varepsilon_{n-1}^{\text{ch}} - \varepsilon_n^{\text{ch}} - \omega) + \delta(\omega + \varepsilon_{n-1}^{\text{ch}} - \varepsilon_n^{\text{ch}})] \\ &\quad - (n+1) [\Theta(\varepsilon_{n+1}^{\text{ch}}) - \Theta(\varepsilon_n^{\text{ch}})] [\delta(\varepsilon_{n+1}^{\text{ch}} - \varepsilon_n^{\text{ch}} - \omega) + \delta(\omega + \varepsilon_{n+1}^{\text{ch}} - \varepsilon_n^{\text{ch}})] \}. \end{aligned} \quad (25)$$

In the first term of Eq. (25), we shift the Landau-level index according to $n \rightarrow n + 1$. This allows both contributions to be combined. Also, by exploiting the linear dispersion of chiral Landau levels, the above expression simplifies to

$$\begin{aligned} \beta^{xxz}(\omega) &= \frac{2\eta e^3}{4\pi \ell_B^2 \omega^2} \left(\sqrt{2} t_{\parallel} \frac{\ell_B}{\hbar} \right)^2 (t_z - v_z \eta) \sum_{n=0}^{\nu-1} (n+1) \\ &\quad \times \int_{-\infty}^{\infty} dk_z [\Theta(\varepsilon_n^{\text{ch}}) - \Theta(\varepsilon_{n+1}^{\text{ch}})] \\ &\quad \times [\delta(\varepsilon_n^{\text{ch}} - \varepsilon_{n+1}^{\text{ch}} - \omega) + \delta(\omega + \varepsilon_n^{\text{ch}} - \varepsilon_{n+1}^{\text{ch}})], \end{aligned} \quad (26)$$

$$\begin{aligned} \beta^{xyz}(\omega) &= i \frac{2\eta e^3}{4\pi \ell_B^2 \omega^2} \left(\sqrt{2} t_{\parallel} \frac{\ell_B}{\hbar} \right)^2 (t_z - v_z \eta) \sum_{n=0}^{\nu-1} (n+1) \\ &\quad \times \int_{-\infty}^{\infty} dk_z [\Theta(\varepsilon_n^{\text{ch}}) - \Theta(\varepsilon_{n+1}^{\text{ch}})] \\ &\quad \times [\delta(\varepsilon_n^{\text{ch}} - \varepsilon_{n+1}^{\text{ch}} - \omega) - \delta(\omega + \varepsilon_n^{\text{ch}} - \varepsilon_{n+1}^{\text{ch}})]. \end{aligned} \quad (27)$$

For chiral Landau levels, the energy difference is independent of k_z and given by $\varepsilon_{n+1} - \varepsilon_n = 2t_{\parallel}$. Carrying out the k_z integration and summation over the m chiral modes, we finally obtain the closed-form expression

$$\left. \begin{aligned} \text{Re} [\beta^{xxz}(\omega)] &= -\frac{e^3}{\hbar} \frac{\eta t_{\parallel}^3}{\pi \hbar^2 \omega^2} \nu(\nu+1) \\ &\quad \times [\delta(\omega - 2t_{\parallel}) + \delta(\omega + 2t_{\parallel})], \\ \text{Im} [\beta^{xyz}(\omega)] &= \frac{e^3}{\hbar} \frac{\eta t_{\parallel}^3}{\pi \hbar^2 \omega^2} \nu(\nu+1) \\ &\quad \times [\delta(\omega - 2t_{\parallel}) + \delta(\omega + 2t_{\parallel})]. \end{aligned} \right\} \quad (28)$$

with a condition set on μ where $\mu > 1$ Equation (28) provides

a remarkably compact closed-form expression for the purely chiral contribution to the second-order optical conductivity tensor^{43,44}. Since only transitions within the chiral Landau-level manifold are involved, the nonlinear response is sharply localized at the resonant frequencies $\omega = \pm 2t_{\parallel}$, as enforced by the Dirac delta functions. These peaks reflect the strict optical selection rules of the chiral sector and highlight the absence of any broad continuum contribution in this channel. Furthermore, the prefactor scales as $\nu(\nu+1)$, demonstrating that the magnitude of the chiral nonlinear response is strongly enhanced for higher-order multi-Weyl nodes. The opposite signs and the separation into $\text{Re} [\beta^{xxz}]$ and $\text{Im} [\beta^{xyz}]$ emphasize the distinct longitudinal and Hall-like character of the second-order response, with the imaginary part capturing the purely antisymmetric nonlinear Hall component. Overall, this result establishes that chiral-to-chiral transitions generate universal and topologically amplified resonant features in the nonlinear magneto-optical conductivity of multi-Weyl semimetals.

B. Chiral-bulk contribution to the injection current

We now consider the contribution to the nonlinear injection current arising from transitions between chiral Landau levels and bulk Landau levels²⁰. In this case, the initial or final state corresponds to a chiral Landau level, denoted by $|n\rangle$, while the intermediate state belongs to the bulk spectrum and is represented by $|n, s\rangle$, where $s = \pm$ labels the band index. The relevant triple current matrix element for this process is given by

$$\begin{aligned} \mathcal{Z}_{n_1 n_2 n_3}^{\alpha \beta z} &= \langle n_3, s_3 | \hat{j}^{\alpha} | n_1 \rangle \langle n_1 | \hat{j}^{\beta} | n_2, s_2 \rangle \\ &\quad \times \langle n_2, s_2 | \hat{j}^z | n_3, s_3 \rangle. \end{aligned} \quad (29)$$

We first evaluate the longitudinal current matrix element

between bulk states,

$$\begin{aligned} \langle n_2, s_2 | \hat{j}^z | n_3, s_3 \rangle &= \begin{pmatrix} u_{n_2, \uparrow}^{s_2} \phi_{n_2-\nu} \\ u_{n_2, \downarrow}^{s_2} \phi_{n_2} \end{pmatrix}^\dagger \begin{pmatrix} t_z + v_z \eta & 0 \\ 0 & t_z - v_z \eta \end{pmatrix} \\ &\quad \times \begin{pmatrix} u_{n_3, \uparrow}^{s_3} \phi_{n_3-\nu} \\ u_{n_3, \downarrow}^{s_3} \phi_{n_3} \end{pmatrix} \\ &= \left[|u_{n_2, \uparrow}^{s_2}|^2 (t_z + v_z \eta) + |u_{n_2, \downarrow}^{s_2}|^2 (t_z - v_z \eta) \right] \\ &\quad \times \delta_{(n_2, s_2), (n_3, s_3)}. \end{aligned} \quad (30)$$

This ensures that the state $|n_2, s_2\rangle = |n_3, s_3\rangle$ and can be written $|\nu, s\rangle$ indicating a bulk state. The relevant triple current matrix element for this process is now given by

$$\mathcal{Z}_{\nu-1, (\nu, s)(\nu, s)}^{xxz} = \langle \nu, s | \hat{j}^x | \nu - 1 \rangle \langle \nu - 1 | \hat{j}^x | \nu, s \rangle \langle \nu, s | \hat{j}^z | \nu, s \rangle \quad (31)$$

$$\mathcal{Z}_{\nu-1, (\nu, s)(\nu, s)}^{xyz} = \langle \nu, s | \hat{j}^x | \nu - 1 \rangle \langle \nu - 1 | \hat{j}^y | \nu, s \rangle \langle \nu, s | \hat{j}^z | \nu, s \rangle \quad (32)$$

The x and y -components of the current matrix element between a bulk and a chiral state become

$$\begin{aligned} \langle \nu, s | \hat{j}^x | \nu - 1 \rangle &= \frac{\ell_B}{\hbar} \begin{pmatrix} u_{\nu, \uparrow}^s \phi_0 \\ u_{\nu, \downarrow}^s \phi_\nu \end{pmatrix}^\dagger \begin{pmatrix} \sqrt{2}t_{\parallel}(\hat{a} + \hat{a}^\dagger) & \frac{\nu}{\sqrt{2}}\tilde{\lambda}_\nu(\hat{a})^{\nu-1} \\ \frac{\nu}{\sqrt{2}}\tilde{\lambda}_\nu(\hat{a}^\dagger)^{\nu-1} & \sqrt{2}t_{\parallel}(\hat{a} + \hat{a}^\dagger) \end{pmatrix} \\ &\quad \times \begin{pmatrix} 0 \\ \phi_{\nu-1} \end{pmatrix} \\ &= \frac{\ell_B}{\hbar} \begin{pmatrix} u_{\nu, \uparrow}^s \phi_0 \\ u_{\nu, \downarrow}^s \phi_\nu \end{pmatrix}^\dagger \begin{pmatrix} \frac{\nu}{\sqrt{2}}\tilde{\lambda}_\nu\sqrt{(\nu-1)!}\phi_0 \\ \sqrt{2}t_{\parallel}\sqrt{\nu}\phi_\nu \end{pmatrix} \\ &= \frac{\ell_B}{\hbar} \left[u_{\nu, \uparrow}^s \frac{\nu}{\sqrt{2}}\tilde{\lambda}_\nu\sqrt{(\nu-1)!} + \sqrt{2}t_{\parallel}u_{\nu, \downarrow}^s\sqrt{\nu} \right], \end{aligned} \quad (33)$$

$$\begin{aligned} \langle \nu, s | \hat{j}^y | \nu - 1 \rangle &= \frac{i\ell_B}{\hbar} \begin{pmatrix} u_{\nu, \uparrow}^s \phi_0 \\ u_{\nu, \downarrow}^s \phi_\nu \end{pmatrix}^\dagger \begin{pmatrix} \sqrt{2}t_{\parallel}(\hat{a} + \hat{a}^\dagger) & -\frac{\nu}{\sqrt{2}}\tilde{\lambda}_\nu\sqrt{(\nu-1)!}\phi_0 \\ \frac{\nu}{\sqrt{2}}\tilde{\lambda}_\nu(\hat{a}^\dagger)^{\nu-1} & \sqrt{2}t_{\parallel}\sqrt{\nu}\phi_\nu \end{pmatrix} \\ &= \frac{i\ell_B}{\hbar} \left[-u_{\nu, \uparrow}^s \frac{\nu}{\sqrt{2}}\tilde{\lambda}_\nu\sqrt{(\nu-1)!} + \sqrt{2}t_{\parallel}u_{\nu, \downarrow}^s\sqrt{\nu} \right]. \end{aligned} \quad (34)$$

Equations (33) and (34) fully determine the chiral-bulk matrix elements entering the nonlinear conductivity. The resulting selection rules show that chiral-bulk transitions connect adjacent Landau levels and explicitly depend on the multi-Weyl node order through the factor $\tilde{\lambda}_\nu$. These contributions are therefore absent in conventional Weyl semimetals ($m = 1$) and constitute a distinct signature of higher-order topology.

$$\langle \nu, s | \hat{j}^y | \nu - 1 \rangle = -\langle \nu - 1 | \hat{j}^y | \nu, s \rangle^*. \quad (35)$$

$$\langle \nu, s | \hat{j}^x | \nu - 1 \rangle = \langle \nu - 1 | \hat{j}^x | \nu, s \rangle^*. \quad (36)$$

This antisymmetry ensures that the xxz and yyz components are equal, $\mathcal{Z}_{n_1 n_2 n_3}^{xxz} = \mathcal{Z}_{n_1 n_2 n_3}^{yyz}$. Combining Eqs. (33, 34 & 35), the triple current correlator entering the nonlinear response takes the form

$$\begin{aligned} \mathcal{Z}_{\nu-1, (\nu, s)(\nu, s)}^{xxz} &= \left(\frac{\ell_B}{\hbar} \left[u_{\nu, \uparrow}^s \frac{\nu}{\sqrt{2}}\tilde{\lambda}_\nu\sqrt{(\nu-1)!} + \sqrt{2}t_{\parallel}u_{\nu, \downarrow}^s\sqrt{\nu} \right] \right)^2 \\ &\quad \times \left[|u_{\nu, \uparrow}^s|^2 (t_z + v_z \eta) + |u_{\nu, \downarrow}^s|^2 (t_z - v_z \eta) \right], \end{aligned} \quad (37)$$

$$\begin{aligned} \mathcal{Z}_{\nu-1, (\nu, s)(\nu, s)}^{xyz} &= i \left(\frac{\ell_B}{\hbar} \left[u_{\nu, \uparrow}^s \frac{\nu}{\sqrt{2}}\tilde{\lambda}_\nu\sqrt{(\nu-1)!} - \sqrt{2}t_{\parallel}u_{\nu, \downarrow}^s\sqrt{\nu} \right] \right)^2 \\ &\quad \times \left[|u_{\nu, \uparrow}^s|^2 (t_z + v_z \eta) + |u_{\nu, \downarrow}^s|^2 (t_z - v_z \eta) \right]. \end{aligned} \quad (38)$$

Substituting the above Eqs. into the general expression for the injection current, Eq. (20), we obtain

$$\begin{aligned} \beta^{xxz}(\omega) &= \frac{\eta}{4\pi\ell_B^2\omega^2} \sum_s \int_{-\infty}^{\infty} dk_z [\Theta(\varepsilon_{\nu, s}^{\text{bulk}}) - \Theta(\varepsilon_{\nu-1}^{\text{ch}})] \mathcal{Z}_{\nu-1, (\nu, s)(\nu, s)}^{xxz} \left[\delta(\varepsilon_{\nu, s}^{\text{bulk}} - \varepsilon_{\nu-1}^{\text{ch}} - \hbar\omega) + \delta(\hbar\omega + \varepsilon_{\nu, s}^{\text{bulk}} - \varepsilon_{\nu-1}^{\text{ch}}) \right], \\ \beta^{xyz}(\omega) &= \frac{i\eta}{4\pi\ell_B^2\omega^2} \sum_s \int_{-\infty}^{\infty} dk_z [\Theta(\varepsilon_{\nu, s}^{\text{bulk}}) - \Theta(\varepsilon_{\nu-1}^{\text{ch}})] \mathcal{Z}_{\nu-1, (\nu, s)(\nu, s)}^{xyz} \left[\delta(\varepsilon_{\nu, s}^{\text{bulk}} - \varepsilon_{\nu-1}^{\text{ch}} - \hbar\omega) - \delta(\hbar\omega + \varepsilon_{\nu, s}^{\text{bulk}} - \varepsilon_{\nu-1}^{\text{ch}}) \right]. \end{aligned} \quad (39)$$

Equation (39) represents the contribution to the nonlinear optical response arising from transitions between the chiral Landau level and the first bulk Landau level²⁷. The difference of the step functions, $[\Theta(\varepsilon_{\nu, s}^{\text{bulk}}) - \Theta(\varepsilon_{\nu-1}^{\text{ch}})]$, ensures that only optically allowed processes consistent with the occupation of initial and final states are included. The quantities \mathcal{Z}^{xxz} and \mathcal{Z}^{xyz} encode the corresponding triple current matrix elements, thereby capturing the strength of the interband coupling between chiral and bulk sectors. The Dirac delta

functions enforce energy conservation for photon absorption and emission processes, with the symmetric and antisymmetric combinations distinguishing the longitudinal component β^{xxz} from the Hall-like component β^{xyz} . This form highlights how the interplay between chiral and bulk Landau levels governs the frequency-dependent nonlinear conductivity in multi-Weyl semimetals.

C. Bulk-bulk contribution

With similar argument, we have, the term to consider as

$$\mathcal{Z}_{(n_1, s_1), (n_2, s_2)(n_2, s_2)}^{xxz} = \langle n_2, s_2 | \hat{j}^x | n_1, s_1 \rangle \langle n_1, s_1 | \hat{j}^x | n_2, s_2 \rangle \langle n_2, s_2 | \hat{j}^z | n_2, s_2 \rangle \quad (40)$$

$$\mathcal{Z}_{(n_1, s_1), (n_2, s_2)(n_2, s_2)}^{xyz} = \langle n_2, s_2 | \hat{j}^x | n_1, s_1 \rangle \langle n_1, s_1 | \hat{j}^y | n_2, s_2 \rangle \langle n_2, s_2 | \hat{j}^z | n_2, s_2 \rangle \quad (41)$$

The matrix element $\langle n_2, s_2 | \hat{j}_x | n_1, s_1 \rangle$ can be written as

$$\langle n_2, s_2 | \hat{j}_x | n_1, s_1 \rangle = e \left(\frac{\ell_B}{\hbar} \right) \{ \mathcal{M}_{n_1, n_2, s_1, s_2} \delta_{n_2, n_1-1} + \mathcal{M}_{n_1-1, n_2, s_1, s_2} \delta_{n_2, n_1-1} \} \quad (42)$$

where we have defined $\mathcal{M}_{n_1, n_2, s_1, s_2} = [\sqrt{2} t_{\parallel} u_{n_1, \uparrow}^{s_1} u_{n_2, \uparrow}^{s_2} \sqrt{n_1 - \nu + 1} + \frac{\nu}{\sqrt{2}} \tilde{\lambda}_{\nu} u_{n_1, \downarrow}^{s_1} u_{n_2, \uparrow}^{s_2} \sqrt{\frac{n_1!}{(n_1 - \nu + 1)!}} + \sqrt{2} t_{\parallel} u_{n_1, \downarrow}^{s_1} u_{n_2, \downarrow}^{s_2} \sqrt{n_1 + 1}]$. Analogously, we can write

$$\langle n_1, s_1 | \hat{j}^y | n_3, s_2 \rangle = ie \left(\frac{\ell_B}{\hbar} \right) \{ -\mathcal{M}_{n_1, n_2, s_1, s_2} \delta_{n_2, n_1-1} + \mathcal{M}_{n_1-1, n_2, s_1, s_2} \delta_{n_2, n_1-1} \} \quad (43)$$

After enforcing the selection rules, the xxz and xyz tensor components are equal and can be written as

$$\begin{aligned} \mathcal{Z}_{(n_1, s_1), (n_2, s_2)(n_2, s_2)}^{xxz} &= e^3 \left(\frac{\ell_B}{\hbar} \right)^2 \{ \mathcal{M}_{n_1, n_2, s_1, s_2} \delta_{n_2, n_1-1} + \mathcal{M}_{n_1-1, n_2, s_1, s_2} \delta_{n_2, n_1+1} \} \\ &\times \{ \mathcal{M}_{n_2, n_1, s_2, s_1} \delta_{n_1, n_2-1} + \mathcal{M}_{n_2-1, n_1, s_2, s_1} \delta_{n_1, n_2+1} \} \left[|u_{n_2, \uparrow}^{s_2}|^2 (t_z + v_z \eta) + |u_{n_2, \downarrow}^{s_2}|^2 (t_z - v_z \eta) \right] \delta_{(n_2, s_2), (n_3, s_3)}. \\ &= e^3 \left(\frac{\ell_B}{\hbar} \right)^2 \{ (\mathcal{M}_{n_1, n_2, s_1, s_2})^2 \delta_{n_2, n_1-1} + (\mathcal{M}_{n_1-1, n_2, s_1, s_2})^2 \delta_{n_2, n_1+1} \} \left[|u_{n_2, \uparrow}^{s_2}|^2 (t_z + v_z \eta) + |u_{n_2, \downarrow}^{s_2}|^2 (t_z - v_z \eta) \right]. \end{aligned} \quad (44)$$

$$\begin{aligned} \mathcal{Z}_{(n_1, s_1), (n_2, s_2)(n_2, s_2)}^{xyz} &= ie^3 \left(\frac{\ell_B}{\hbar} \right)^2 \{ (\mathcal{M}_{n_1, n_2, s_1, s_2}) \delta_{n_2, n_1-1} + \mathcal{M}_{n_1-1, n_2, s_1, s_2} \delta_{n_2, n_1+1} \} \\ &\times \{ -\mathcal{M}_{n_2, n_1, s_2, s_1} \delta_{n_1, n_2-1} + \mathcal{M}_{n_2-1, n_1, s_2, s_1} \delta_{n_1, n_2+1} \} \left[|u_{n_2, \uparrow}^{s_2}|^2 (t_z + v_z \eta) + |u_{n_2, \downarrow}^{s_2}|^2 (t_z - v_z \eta) \right] \delta_{(n_2, s_2), (n_3, s_3)} \\ &= ie^3 \left(\frac{\ell_B}{\hbar} \right)^2 \{ (\mathcal{M}_{n_1-1, n_2, s_1, s_2})^2 \delta_{n_2, n_1+1} - (\mathcal{M}_{n_1, n_2, s_1, s_2})^2 \delta_{n_2, n_1-1} \} \left[|u_{n_2, \uparrow}^{s_2}|^2 (t_z + v_z \eta) + |u_{n_2, \downarrow}^{s_2}|^2 (t_z - v_z \eta) \right]. \end{aligned} \quad (45)$$

Substituting Eqs. (44) and (45) into the general expression for the second-order response yields

$$\left. \begin{aligned} \beta^{xxz} &= \frac{\eta e^3}{4\pi\ell_B^2\omega^2} v_z \left(\frac{\ell_B}{\hbar} \right)^2 \sum_{s \neq s'} \int_{-\infty}^{\infty} dk_z \left[\Theta(\varepsilon_{n+1, s'}^{\text{bulk}}) - \Theta(\varepsilon_{n, s}^{\text{bulk}}) \right] \mathcal{M}_{n, n+1, s, s'} \\ &\times \left(|u_{n+1, \uparrow}^{s'}|^2 - |u_{n, \uparrow}^s|^2 - |u_{n+1, \downarrow}^{s'}|^2 + |u_{n, \downarrow}^s|^2 \right) \left\{ \delta(-\varepsilon_{n, s}^{\text{bulk}} + \varepsilon_{n+1, s'}^{\text{bulk}} + \omega) + \delta(-\omega - (\varepsilon_{n, s}^{\text{bulk}} - \varepsilon_{n+1, s'}^{\text{bulk}})) \right\}, \\ \beta^{xyz} &= i \frac{\eta e^3}{4\pi\ell_B^2\omega^2} v_z \left(\frac{\ell_B}{\hbar} \right)^2 \sum_{s \neq s'} \int_{-\infty}^{\infty} dk_z \left[\Theta(\varepsilon_{n+1, s'}^{\text{bulk}}) - \Theta(\varepsilon_{n, s}^{\text{bulk}}) \right] \mathcal{M}_{n, n+1, s, s'} \\ &\times \left(|u_{n+1, \uparrow}^{s'}|^2 - |u_{n, \uparrow}^s|^2 - |u_{n+1, \downarrow}^{s'}|^2 + |u_{n, \downarrow}^s|^2 \right) \left\{ \delta(-\varepsilon_{n, s}^{\text{bulk}} + \varepsilon_{n+1, s'}^{\text{bulk}} + \omega) - \delta(-\omega - (\varepsilon_{n, s}^{\text{bulk}} - \varepsilon_{n+1, s'}^{\text{bulk}})) \right\}. \end{aligned} \right\} \quad (46)$$

Using the analytical expressions derived in the previous sections, we now present the full frequency-dependent nonlinear response of multi-Weyl semimetals in the presence of a perpendicular magnetic field. Figure 1 displays the behavior of the Hall-like component $\text{Im}[\beta^{xyz}(\omega)]$ and the longitudinal component $\text{Re}[\beta^{xxz}(\omega)]$ for different winding numbers $\nu = 1, 2$, and 3, and for several values of the chemical potential μ .

The total nonlinear conductivity is obtained by incorporating all relevant Landau-level transition channels^{27,31,46,48-55}. In particular, the contribution arising purely from chiral

Landau-level transitions is governed by the compact closed-form result in Eq. (28), which produces distinct low-energy resonances associated with the chiral sector. In addition, mixed transitions between the chiral level and higher bulk Landau levels are captured by Eq. (39), leading to additional peaks and threshold structures in the intermediate-frequency regime. Finally, the dominant high-energy response originates from bulk-to-bulk interband processes described by Eq. (46), which become increasingly prominent as more bulk Landau levels participate in optical transitions.

As evident from Fig. 1, the nonlinear response exhibits a

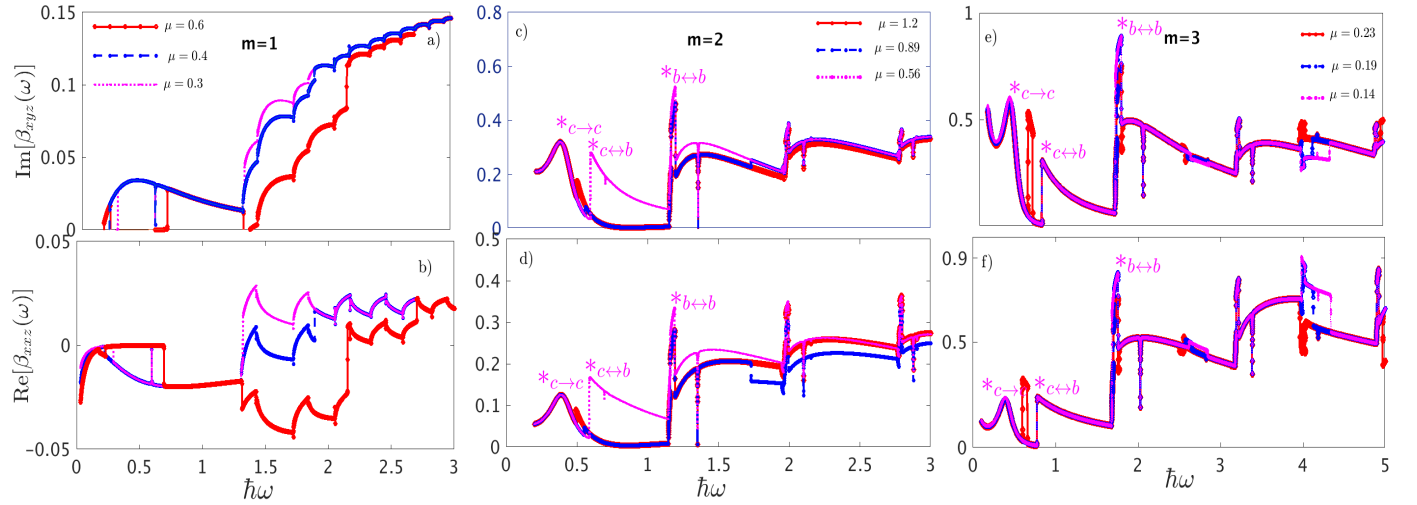


FIG. 1. The components of second-order DC conductivities β^{xyz} and β^{xxz} (in the units of $\frac{e^3}{\hbar}$) as a function of the photon energy $\hbar\omega$. The plots are obtained for multi-Weyl nodes with finite tilting parameters ($t_{\parallel}, t_z \neq 0$) where chiral to chiral transitions becomes significant. The various curves illustrate the behaviour at different chemical potential.

series of sharp resonant features and step-like variations, reflecting the energy-conserving delta-function selection rules imposed by Landau-level quantization. The onset of the spectra at low photon energies is primarily dictated by chiral-to-chiral ($c \rightarrow c$) transitions, which provide the leading contribution in the vicinity of the chiral Landau level. With increasing frequency, additional absorption thresholds emerge from chiral-to-bulk ($c \rightarrow b$) processes, marking the activation of transitions between the topologically protected chiral mode and the first bulk Landau levels. At still higher energies, the response becomes dominated by bulk-to-bulk ($b \rightarrow b$) interband transitions, resulting in multiple resonant peaks as successive bulk Landau levels enter the optical window.

Moreover, the overall magnitude and complexity of the spectra increase systematically with the winding number ν , demonstrating that higher-order Weyl nodes significantly enhance the nonlinear magneto-optical conductivity through the interplay of chiral and bulk excitations.

D. Nonlinear Magneto-Optical Response in the Untilting Limit

In this section we evaluate the second-order optical conductivity tensor for multi-Weyl semimetals in the absence of tilting. We set the in-plane and out-of-plane tilt parameters to zero, i.e., $t_{\parallel} = 0$ and $w_z = 0$, so that the Landau-level spectrum remains fully symmetric about the Weyl node. This limit is particularly important because it allows the nonlinear optical tensor to be expressed in a closed and compact analytical form. In the presence of tilt, the Landau-level structure becomes asymmetric and the resulting nonlinear response generally involves complicated energy dispersions, making it difficult to obtain transparent expressions beyond numerical evaluation.

By focusing on the untilted case, we are able to isolate the intrinsic topological contribution of multi-Weyl nodes and derive simplified results for the second-order conductivity com-

ponents in terms of a few universal parameters. Such compact formulas provide direct physical insight into the role of chiral Landau levels and optical selection rules, and serve as a useful reference point for understanding how additional effects, such as tilting or disorder, modify the nonlinear magneto-optical response.

Bulk-bulk nonlinear response in the untilting limit: In this limit, the Landau-level spectrum becomes symmetric about the Weyl node, and the bulk Landau-level energies reduce to s -dependent branches of the form $\varepsilon_{n,s}^{\text{bulk}}(k_z) = s\Gamma_n^{\nu}(k_z)$. As a result, the band index $s = \pm$ directly labels electron- and hole-like states, and optical transitions contributing to the nonlinear response are restricted to interband processes with $s \neq s'$. The absence of tilt considerably simplifies the structure of the current matrix elements. In particular, the difference of spinor weights appearing in Eq. (46), $|u_{n+1,\uparrow}^{s'}|^2 - |u_{n,\uparrow}^s|^2 - |u_{n+1,\downarrow}^{s'}|^2 + |u_{n,\downarrow}^s|^2$, can be expressed solely in terms of the Landau-level energies $\Gamma_n^{\nu}(k_z)$ and $\Gamma_{n+1}^{\nu}(k_z)$. This cancellation reflects the restoration of particle-hole symmetry in the untilted Hamiltonian and ensures that only interband coherence contributes to the second-order optical response^{15,16}. The delta functions in Eq. (46) enforce energy conservation for optical transitions between adjacent bulk Landau levels, $\varepsilon_{n+1,s'}^{\text{bulk}}(k_z) - \varepsilon_{n,s}^{\text{bulk}}(k_z) = \pm\hbar\omega$. Since $\Gamma_n^{\nu}(k_z)$ depends quadratically on k_z , these constraints define two symmetric roots in k_z , which allows the momentum integral to be evaluated analytically. Carrying out the k_z integration converts the delta functions into inverse Jacobian factors, producing the characteristic square-root structure associated with the one-dimensional joint density of states along the magnetic-field direction. The difference between the longitudinal component β^{xxz} and the Hall-type component β^{xyz} arises entirely from the relative sign between the two delta-function contributions in Eq. (46). While both components share the same resonance structure, this sign difference leads to qualitatively distinct frequency dependences: β^{xyz} acquires an imaginary prefactor and is odd under time-reversal, whereas β^{xxz} remains purely real. Collecting all contribu-

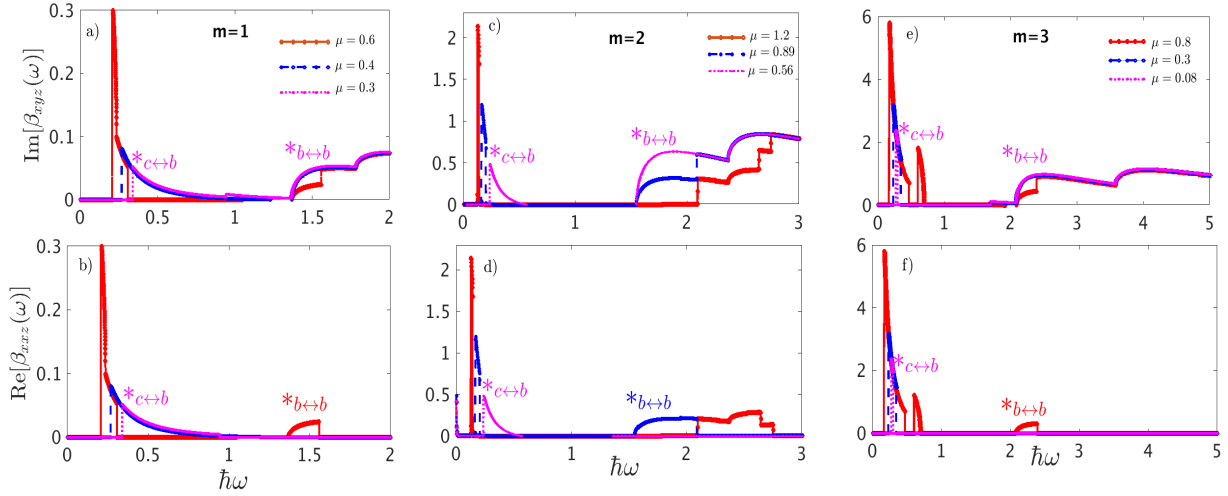


FIG. 2. The photon-energy dependence of the second-order DC conductivity components β^{xyz} and β^{xxz} (in units of e^3/\hbar) is presented for multi-Weyl nodes in the untilted limit ($t_{\parallel} = 0, t_z = 0$), as derived from Eqs. (47) and (50). The individual curves correspond to different chemical potentials.

tions, we arrive at the closed-form expressions for the nonlin-

ear bulk-bulk response in the untilting limit, presented below.

$$\left. \begin{aligned} \beta^{xyz}(\omega) &= i \frac{e^3}{\hbar} \frac{\varepsilon_B^2 f^2(\nu, n)}{8\pi [\omega^4 - (\varepsilon_B f(\nu, n))^4]} \sum_n \left[\Theta(\omega^2 + f^2(\nu, n) \varepsilon_B^2 - |2\mu\omega|) \right. \\ &\quad \left. + \text{sgn}[\Theta(\omega^2 - f^2(\nu, n) \varepsilon_B^2 - |2\mu\omega|)] \sqrt{f^4(\nu, n) \varepsilon_B^4 + (\hbar\omega)^4 - 2(\hbar\omega)^2 \varepsilon_B^2 g^2(\nu, n)} \right], \\ \beta^{xxz}(\omega) &= \frac{e^3}{\hbar} \frac{\varepsilon_B^2 f^2(\nu, n)}{8\pi [\omega^4 - (\varepsilon_B f(\nu, n))^4]} \sum_n \left[\Theta(\omega^2 + f^2(\nu, n) \varepsilon_B^2 - |2\mu\omega|) \right. \\ &\quad \left. - \Theta(\omega^2 - f^2(\nu, n) \varepsilon_B^2 - |2\mu\omega|) \sqrt{f^4(\nu, n) \varepsilon_B^4 + (\hbar\omega)^4 - 2(\hbar\omega)^2 \varepsilon_B^2 g^2(\nu, n)} \right]. \end{aligned} \right\} \quad (47)$$

where the structure functions $f(\nu, n)$ and $g(\nu, n)$ are defined as

$$g^2(\nu, n) = \frac{2(n+1)-\nu}{n-\nu+1} \frac{n!}{(n-\nu)!}, \quad (48)$$

$$f^2(\nu, n) = \frac{-\nu n!}{(n+1-\nu)(n-\nu)}. \quad (49)$$

These functions encode the dependence of the nonlinear response on the topological charge of the Weyl node and the Landau-level index. The step functions Θ restrict the transitions to those satisfying the optical selection rules, while the square-root term represents the joint density of states for allowed transitions.

Chiral to bulk transitions. In the absence of tilt, the longitudinal current matrix element entering $\mathcal{Z}_{\nu-1,(\nu,s)(\nu,s)}$ reduces to a purely velocity-dependent factor, while the transverse matrix elements depend only on the multi-Weyl coupling $\tilde{\lambda}_{\nu}$. Consequently, the triple current correlator factorizes into an energy-dependent prefactor multiplied by a monopole-charge-dependent constant. This allows the chiral-bulk response to

be expressed entirely in terms of the magnetic energy scale ε_B and the monopole charge ν .

The delta functions in Eq. (39) enforce energy conservation for optical transitions between the chiral and bulk Landau levels,

$$\varepsilon_{\nu,s}^{\text{bulk}}(k_z) - \varepsilon_{\nu-1}^{\text{ch}}(k_z) = \pm \hbar\omega.$$

Since $\Gamma_{\nu}^{\nu}(k_z)$ depends quadratically on k_z , this constraint defines symmetric roots in momentum space, allowing the k_z integration to be performed analytically. Carrying out the integration converts the delta functions into inverse Jacobian factors, producing a characteristic rational frequency dependence that is distinct from the bulk-bulk response.

After evaluating the k_z integral and summing over the bulk band index s , the nonlinear response assumes a universal form governed by a single structure function $f(\nu) = \nu!$. The difference between the longitudinal component β^{xxz} and the Hall-type component β^{xyz} arises from the relative sign between the two delta-function contributions in Eq. (39). While both components share identical resonance conditions, β^{xyz} acquires an imaginary prefactor and is odd under time-reversal symmetry, whereas β^{xxz} remains purely real.

Collecting all contributions, we obtain the closed-form expressions for the chiral-bulk nonlinear injection current in the untilting limit. These results reveal a pronounced low-

frequency enhancement controlled by the topological chiral Landau level and provide a direct nonlinear optical signature of the multi-Weyl monopole charge.

$$\left. \begin{aligned} \beta^{xyz}(\omega) &= i \frac{e^3}{\hbar} \frac{\varepsilon_B^2 f^2(\nu) \nu}{16\pi\omega^2} \left[\Theta(\omega^2 + f^2(\nu)\varepsilon_B^2 - |2\mu\omega|) + \text{sgn} \left[\Theta(\omega^2 - f^2(\nu)\varepsilon_B^2 - |2\mu\omega|) \right] \frac{-\omega^2 + f^2(\nu)\varepsilon_B^2 \nu}{\omega^2 + f^2(\nu)\varepsilon_B^2 \nu} \right], \\ \beta^{xxz}(\omega) &= \frac{e^3}{\hbar} \frac{\varepsilon_B^2 f^2(\nu) \nu}{16\pi\omega^2} \left[\Theta(\omega^2 + f^2(\nu)\varepsilon_B^2 - |2\mu\omega|) - \Theta(\omega^2 - f^2(\nu)\varepsilon_B^2 - |2\mu\omega|) \frac{-\omega^2 + f^2(\nu)\varepsilon_B^2 \nu}{\omega^2 + f^2(\nu)\varepsilon_B^2 \nu} \right], \end{aligned} \right\} \quad (50)$$

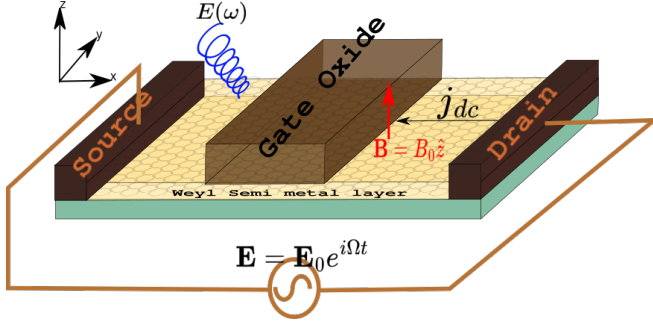


FIG. 3. Schematic of a gated transport geometry for detecting nonlinear magneto-optical injection currents in a multi-Weyl semimetal. A multi-Weyl channel is contacted by metallic source and drain electrodes and electrostatically tuned through a gate oxide layer. A perpendicular magnetic field $\mathbf{B} = B_0 \hat{z}$ quantizes the spectrum into chiral and bulk Landau levels, while illumination by a circularly polarized optical field $E(\omega) = E_0 e^{i\Omega t}$ drives resonant inter-Landau level transitions. The resulting asymmetric carrier population generates a dc photocurrent j_{dc} along the channel, providing a direct transport probe of the second-order injection tensor $\beta^{\alpha\beta\gamma}(\omega)$ and its characteristic chiral-chiral, chiral-bulk, and bulk-bulk contributions discussed in the paper.

with $f^2(\nu) = \nu!$. The chiral-bulk contribution is particularly significant at low frequencies, since it directly reflects the topological character of the chiral Landau level and its coupling to the electromagnetic field.

Experimental relevance and gated device geometry: The nonlinear magneto-optical injection current derived in this work can be probed in a gated transport configuration closely analogous to a field-effect transistor geometry, where a multi-Weyl semimetal forms the conducting channel between metallic source and drain contacts and is electrostatically tuned by a gate electrode separated through an insulating oxide layer. In the presence of a perpendicular magnetic field $\mathbf{B} = B_0 \hat{z}$, the electronic spectrum is quantized into bulk and chiral Landau levels, providing the microscopic origin of the frequency-selective resonances identified in the second-order conductivity tensor. Illumination by a circularly polarized optical field $E(\omega) = E_0 e^{i\Omega t}$ drives resonant inter-Landau-level transitions whose asymmetric population dynamics generate a dc photocurrent j_{dc} along the channel via the injection mechanism captured by the tensor $\beta^{\alpha\beta\gamma}(\omega)$ ¹. Within this geometry, the gate voltage directly controls the

chemical potential relative to the chiral and bulk Landau levels, enabling experimental isolation of the distinct chiral-chiral, chiral-bulk, and bulk-bulk contributions predicted by the theory, as well as their characteristic monopole-charge scaling and tilt-dependent spectral structure. The resulting source-drain photocurrent therefore provides a direct transport signature of the nonlinear magneto-optical response and offers a realistic route for detecting topological enhancement of injection currents in multi-Weyl semimetals.

IV. CONCLUSIONS

In this work, we developed a comprehensive microscopic theory of nonlinear magneto-optical injection currents in multi-Weyl semimetals subjected to a uniform magnetic field. Starting from a tilted multi-Weyl Hamiltonian with arbitrary monopole charge ν , we derived the full Landau-level spectrum and formulated the second-order conductivity tensor within a Kubo-type nonlinear response framework. This approach enabled a unified treatment of optical transitions involving chiral, mixed chiral-bulk, and bulk Landau levels, thereby revealing the complete structure of the nonlinear magneto-optical response.

Our analysis shows that transitions confined within the chiral Landau-level manifold generate universal resonant peaks sharply localized at frequencies determined solely by the in-plane tilt parameter. The magnitude of this purely topological contribution scales as $\nu(\nu + 1)$, demonstrating a strong enhancement of nonlinear response with increasing Weyl-node order. Mixed chiral-bulk transitions introduce additional intermediate-frequency structures governed by the magnetic energy scale and monopole charge, while bulk-to-bulk processes dominate the high-frequency regime through a sequence of Landau-level resonances and threshold features. Together, these channels produce a characteristic multiscale spectral profile that directly encodes the topology of multi-Weyl nodes.

In the absence of tilt, we obtained compact closed-form analytical expressions for the nonlinear conductivity tensor. These results isolate the intrinsic topological contribution of multi-Weyl semimetals and reveal universal scaling governed by the magnetic energy scale and factorial structure functions associated with higher monopole charge. The distinct behaviors of the longitudinal component $\text{Re}[\beta^{xxz}]$ and the Hall-type component $\text{Im}[\beta^{xyz}]$ further clarify the separation between dispersive and absorptive nonlinear magneto-optical responses.

Overall, our findings establish nonlinear magneto-optical

injection currents as a sensitive probe of higher-order Weyl topology and chiral Landau physics. The predicted resonant structures, monopole-charge scaling, and universal frequency dependences provide clear experimental signatures accessible through terahertz or infrared spectroscopy in candidate multi-Weyl materials. More broadly, this work highlights the power of nonlinear optical responses in strong magnetic fields as a

route toward identifying and characterizing topological quantum matter beyond the linear-response paradigm.

Future directions include the incorporation of disorder and finite relaxation dynamics, extension to finite temperature and interaction effects, and exploration of nonlinear responses in related topological systems such as multifold fermions and pseudospin-1 semimetals.

¹ C. Zeng, S. Nandy, and S. Tewari, “Nonlinear transport in Weyl semimetals induced by Berry curvature dipole”, *Phys. Rev. B* **103**, 245119 (2021)

² X. Wan, A. M. Turner, A. Vishwanath, and S. Y. Savrasov, “Topological semimetal and Fermi-arc surface states in the electronic structure of pyrochlore iridates”, *Phys. Rev. B* **83**, 205101 (2011)

³ S. Nandy, I. Sodemann, “Symmetry and Quantum Kinetics of the Non-linear Hall Effect”, *Phys. Rev. B* **100**, 195117 (2019)

⁴ N. P. Armitage, E. J. Mele, and A. Vishwanath, “Weyl and Dirac semimetals in three-dimensional solids”, *Rev. Mod. Phys.* **90**, 015001 (2018)

⁵ A. A. Burkov and L. Balents, “Weyl Semimetal in a Topological Insulator Multilayer”, *Phys. Rev. Lett.* **107**, 127205 (2011)

⁶ I. Sodemann and L. Fu, “Quantum Nonlinear Hall Effect Induced by Berry Curvature Dipole in Time-Reversal Invariant Materials”, *Phys. Rev. Lett.* **115**, 216806 (2015)

⁷ S. Yang Xu, I. Belopolski, N. Alidoust, M. Neupane, C. Zhang, R. Sankar, S. M. Huang, C. C. Lee, G. Chang, B. Wang, G. Bian, H. Zheng, D. S. Sanchez, F. Chou, H. Lin, S. Jia, M. Z. Hasan, “Discovery of a Weyl Fermion Semimetal and Topological Fermi Arcs”, *Science* **349**, 613-617 (2015)

⁸ B. Q. Lv, H. M. Weng, B. B. Fu, X. P. Wang, H. Miao, J. Ma, P. Richard, X. C. Huang, L.X. Zhao et al, “Experimental Discovery of Weyl Semimetal TaAs”, *Phys. Rev. X* **5**, 031013 (2015)

⁹ G. E. Volovik, “The Universe in a Helium Droplet”, *Oxford University Press, Oxford*, 2003

¹⁰ A. A. Burkov, “Chiral Anomaly and Diffusive Magnetotransport in Weyl Metals”, *Phys. Rev. Lett.* **113**, 247203 (2014)

¹¹ H. B. Nielsen and M. Ninomiya, “The Adler-Bell-Jackiw anomaly and Weyl fermions in a crystal”, *Phys. Lett. B* **130**, 389 (1983)

¹² D. T. Son and B. Z. Spivak, D. T. Son and B. Z. Spivak, “Chiral anomaly and classical negative magnetoresistance of Weyl metals”, *Phys. Rev. B* **88**, 104412 (2013)

¹³ S. Saha, D. Das and A. Mawrie, “Unveiling the chiral states in multi-Weyl semimetals via theoretical investigation of magneto-optical spectroscopy”, *J. Phys.: Condens. Matter* **37** 405702 **37**, 405702(2025)

¹⁴ R. Lin. Chu, W. Yu. Shan, J. Lu, S. Q. Shen, “Surface and Edge States in Topological Semi-metals”, *Phys Review B* **83**, 075110 (2011)

¹⁵ F. de Juan, A. G. Grushin, T. Morimoto & J. E. Moore, “Quantized circular photogalvanic effect in Weyl semimetals”, *Nature Communications* **8**, 15995 (2017)

¹⁶ C. Fang, M. J. Gilbert, X. Dai, and B. A. Bernevig, “Multi-Weyl Topological Semimetals Stabilized by Point Group Symmetry”, *Phys. Rev. Lett.* **108**, 266802 (2012)

¹⁷ S.-S. Gong, W. Zhu, and D. N. Sheng, “Phase diagram of the spin- $1/2 - J_1 - J_2$ Heisenberg model on a honeycomb lattice” *Phys. Rev. B* **88**, 165138 (2013)

¹⁸ K.-Y. Yang, Y.-M. Lu, and Y. Ran, “Quantum Hall effects in a Weyl semimetal: Possible application in pyrochlore iridates”, *Phys. Rev. B* **84**, 075129 (2011)

¹⁹ T. Morimoto and N. Nagaosa, “Topological nature of nonlinear optical effects in solids”, *Sci. Adv.* **2**, (2016)

²⁰ J. E. Moore and J. Orenstein, “Confinement-Induced Berry Phase and Helicity-Dependent Photocurrents”, *Phys. Rev. Lett.* **105**, 026805 (2010) *Phys. Rev. Lett.* **105**, 026805(2010)

²¹ J. E. Sipe and A. I. Shkrebtii, “Second-order optical response in semiconductors”, *Phys. Rev. B* **61**, 5337 (2000)

²² J. I. Facio, D. Efremov, K. Koepernik, J.-S. You, I. I. Mazin, and J. van den Brink, “Strongly enhanced Berry dipole at topological phase transitions in BiTeI”, *Phys. Rev. Lett.* **121**, 246403 (2018)

²³ Q. Ma *et al.*, “Direct optical detection of Weyl fermion chirality in a topological semimetal”, *Nat. Phys.* **13**, 842 (2017)

²⁴ C. K. Chan, N. H. Lindner, G. Refael, and P. A. Lee, “Photocurrents in Weyl semimetals”, *Phys. Rev. B* **95**, 041104 (2017)

²⁵ D. Rees *et al.*, “Helicity-dependent photocurrents in the chiral Weyl semimetal RhSi”, *Sci. Adv.* **6**, 29 (2020)

²⁶ Z. Ni *et al.*, “High-throughput calculations of magnetic topological materials”, *Nature* **586**, 702 (2020)

²⁷ C. J. Tabert and J. P. Carbotte, “Optical conductivity of Weyl semimetals and signatures of the gapped semimetal phase transition”, *Phys. Rev. B* **93**, 085442 (2016).

²⁸ J. P. Carbotte, “Optical response of a line node semimetal”, *J. Phys.: Condens. Matter* **29**, 045301 (2016).

²⁹ P. E. C. Ashby, J. P. Carbotte, “Chiral anomaly and optical absorption in Weyl semimetals”, *Phys. Rev. B* **89**, 245121(2014)

³⁰ Z. Min. Huang, J. Zhou, and S.Q. Shen, “Topological responses from chiral anomaly in multi-Weyl semimetals”, *Phys. Rev. B* **96**, 085201(2017)

³¹ S. Ahn, E. J. Mele, and H. Min1, “Optical conductivity of multi-Weyl semimetals”, *Phys. Rev. B* **95**, 161112(2017)

³² A. A. Zyuzin, R. P. Tiwari , “Intrinsic anomalous Hall effect in type-II Weyl semimetals”, *JETP Lett.* **103**, 717(2016)

³³ A. A. Soluyanov, D. Gresch, Z. Wang, Q Wu, M. Troyer, X. Dai & B. A. Bernevig, “Type-II Weyl Semimetals”, *Nature* **527**, 495-498(2015)

³⁴ D. E. Parker, T. Morimoto1, J Orenstein and J. E. Moore, “Diagrammatic approach to nonlinear optical response with application to Weyl semimetals”, *Phys. Rev. B* **99**, 045121(2019)

³⁵ A. Menon, S. Chattopadhyay and B. Basu, “Chiral magnetic effect in lattice models of tilted multi-Weyl semimetals”, *Phys. Rev. B* **104**, 075129(2021)

³⁶ R. Takahashi, M. Hirayama, and S. Murakami1, “Spinless hourglass nodal-line semimetals”, *Phys. Rev. B* **96**, 155206(2017)

³⁷ B. Q. Lv *et al.*, “Observation of Weyl nodes in TaAs”, *Nat. Phys.* **11**, 724 (2015).

³⁸ S. Y. Xu *et al.*, “Discovery of a Weyl fermion state with Fermi arcs in niobium arsenide,”, *Nat. Phys.* **11**, 748-754 (2015).

³⁹ L. X. Yang *et al.*, “Weyl semimetal phase in the non-centrosymmetric compound TaAs”, *Nat. Phys.* **11**, 728 (2015).

⁴⁰ S.-M. Huang *et al.*, “New type of Weyl semimetal with quadratic doubleWeyl fermions”, *Proc. Natl. Acad. Sci. USA* **113**, 1180 (2015).

⁴¹ P. Tang, Q. Zhou, and S.-C. Zhang, “Multiple types of topological fermions in transition metal silicides”, *Phys. Rev. Lett.* **119**, 206402 (2017).

⁴² N. B. M. Schröter *et al.*, “Topological chiral crystals with multifold band crossings and long Fermi arcs”, *Nat. Phys.* **15**, 759-765 (2019).

⁴³ G. Bednik,V. Kozii, “Magnetic field induces giant nonlinear optical response in Weyl semimetals”, *Phys. Rev. B* **109**, 045106 (2024)

⁴⁴ A. Avdoshkin, V. Kozii1, and J. E. Moore, “Interactions Remove the Quantization of the Chiral Photocurrent at Weyl Points”, *Phys. Rev. Lett.* **124**, 196603(2020)

⁴⁵ A. Bharti, G. Dixit, “Non-perturbative nonlinear optical responses in Weyl semimetals”, *Appl. Phys. Lett***125**, 051104(2024)

⁴⁶ E. J. König, H.-Y. Xie, D. A. Pesin, and A. Levchenko, “Photogalvanic effect in Weyl semimetals”, *Phys. Rev. B* **96**, 075123 – Published 11 August, 2017 **96**, 075123(2017)

⁴⁷ C. Aversa and J. E. Sipe, “Nonlinear optical susceptibilities of semiconductors: Results with a length-gauge analysis”, *Phys. Rev. B* **52**, 14636(1995)

⁴⁸ H. Weng, C. Fang, Z. Fang, B. A. Bernevig, and X. Dai1, “Weyl Semimetal Phase in Noncentrosymmetric Transition-Metal Monophosphides”, *Phys. Rev. X* **5**, 011029 (2015)

⁴⁹ Q. Ma *et al.*, “Observation of the nonlinear Hall effect under time-reversal-symmetric conditions”, *Nature* **565**, 337- (2019)

⁵⁰ H.-Z. Lu and S.-Q. Shen, “Quantum transport in topological semimetals under magnetic fields”, *Front. Phys.* **12**, 127201 (2017)

⁵¹ A. A. Burkov, “Chiral anomaly and transport in Weyl metals”, *J. Phys.: Condens. Matter* **27**, 113201 (2015)

⁵² M. O. Goerbig, “Electronic Properties of Graphene in a Strong Magnetic Field”, *Rev. Mod. Phys.* **83**, 1193 (2011)

⁵³ J. Behrends,S. Roy,M. H. Kolodrubetz, Jens H. Bardarson, and A. G. Grushin4, “Landau levels, Bardeen polynomials, and Fermi arcs in Weyl semimetals: Lattice-based approach to the chiral anomaly”, *Phys. Rev. B* **99**, 140201(2019)

⁵⁴ S M João and J. M. Lopes, “Basis-independent spectral methods for non-linear optical response in arbitrary tight-binding models”, *Journal of Physics: Condensed Matter*, **32**, 125901(2020)

⁵⁵ L. X. Fu and C. M. Wang, “Thermoelectric transport of multi-Weyl semimetals in the quantum limit”, *Phys. Rev. B* **105**, 035201(2022)